Journal of Materials Chemistry C

ROYAL SOCIETY OF CHEMISTRY

PAPER

View Article Online
View Journal | View Issue

Cite this: J. Mater. Chem. C, 2020, 8, 5950

Enhanced dielectric performance in flexible MWCNT/poly(vinylidene fluoride-*co*-hexafluoropropene)-based nanocomposites by designing a tri-layered structure†

Jie Chen,[a] Yifei Wang,[b] Jiufeng Dong,[c] Yujuan Niu,[cd] Weixing Chen[a] and Hong Wang*[c]

Received 10th January 2020,
Accepted 13th March 2020

DOI: 10.1039/d0tc00148a

rsc.li/materials-c

Polymer composites with high permittivity exhibit promising applications in advanced electronics. However, it remains a challenge to simultaneously achieve high permittivity, low dielectric loss, and high flexibility in single layer nanocomposites. In this work, a series of ternary tri-layered structure films is produced *via* a facile solution-casting process. Two outer layers of a poly(vinylidene fluoride-*co*-hexafluoropropene) (P(VDF-HFP)) ferroelectric copolymer matrix are filled with acid-treated multi-walled carbon nanotubes (MWCNTs) to enhance permittivity, while the inner layer of P(VDF-HFP) blended with poly(methyl methacrylate) (PMMA) can effectively suppress the dielectric losses. The acid-treated MWCNT filler, organic–organic blend, and tri-layered structure contribute to the increase of permittivity, decrease of dielectric loss, and favorable mechanical reliability. As a result, the tri-layered composites with an optimized MWCNT content of 9 wt% at a test frequency of 1 kHz have been endowed with a maximized permittivity of 21 and low dielectric loss of 0.05. Specifically, excellent capacitive stability is demonstrated in these trilayered films over straight bending cycles (*i.e.* 20 000 cycles) and winding (*i.e.* 120 hours) tests. These attractive features of the designed tri-layered structure composites manifest that the facile approach proposed herein is scalable and can be extended to develop flexible composites with high permittivity and low dielectric loss for dielectric applications.

1. Introduction

Flexible dielectric polymer composites have gained wide applicability due to their light weight and easy processing, compared with those of traditional dielectric materials, such as mica and silicon dioxide.[1] Dielectric polymer composites with high permittivity are urgently needed for promising applications in advanced electronics,[2–8] such as embedded components, gate dielectrics, electromechanical transducers, energy storage devices, and piezoelectric generators. As a representative polymer matrix, ferroelectric polymer polyvinylidene fluoride (PVDF) can offer a higher permittivity (K = 10–12) than that (K = 2.2, at 1 kHz) of nonpolar polymers, such as polypropylenes (PP) for the state-of-the-art dielectric capacitor films, due to a strong dipole moment in the C–F groups of PVDF molecular chains.[9–12] However, its dielectric losses (tan δ) are higher than those of PP, and are caused by the relaxation of electrical dipoles, which results in generating waste heat that would be bad for the reliability of the dielectric capacitors.[13] Consequently, the chemical structure of PVDF needs to be modified by reducing its cooperative ferroelectricity in the crystals. Hexafluoropropylene (HFP), as a kind of bulky comonomer, can reduce the dielectric loss and the crystallite size when it is randomly incorporated in the PVDF main chain, thus attracting attention for dielectric applications.[14] Nevertheless, the permittivity (K = 8–10) of poly(vinylidene fluoride-*co*-hexafluoropropene) (P(VDF-HFP)) ferroelectric copolymer still does not satisfy the requirements of dielectric performance.[15]

The introduction of high-K ceramic nanofillers, such as titanium oxide (TO),[16,17] barium titanate (BT),[18,19] barium strontium titanate (BST),[20,21] into the ferroelectric copolymer matrix to form polymer nanocomposites is the most popular strategy to increase permittivity of the ferroelectric copolymers.

[a] School of Materials and Chemical Engineering, Xi'an Technological University, Xi'an 710021, China
[b] Electrical Insulation Research Center, Institute of Materials Science, University of Connecticut, Storrs, Connecticut 06269, USA
[c] Department of Materials Science and Engineering & Shenzhen Engineering Research Center for Novel Electronic Information Materials and Devices, Southern University of Science and Technology, Shenzhen 518055, China. E-mail: wangh6@sustech.edu.cn
[d] SUSTech Academy for Advanced Interdisciplinary Studies, Southern University of Science and Technology, Shenzhen 518055, China

† Electronic supplementary information (ESI) available. See DOI: 10.1039/d0tc00148a

Nevertheless, the drawback of the polymer nanocomposite approach is that the high-K ceramic fillers with high filler concentrations (*e.g.* ~50 vol%) inevitably need to obtain a permittivity value of about 50, thus resulting in dramatic worsening of their poor processability, polymer flexibility, elasticity, and dielectric loss.[22]

Preparing percolation composites is another route for increasing the permittivity of composites, where conductive fillers such as metal particles,[23] MXene nanosheets,[24] carbon black,[25] carbon nanotubes[26] or graphene[27] are employed as fillers in the polymer matrix. The permittivity of composites filled with carbon fillers is much higher than those of composites introduced with ceramic fillers due to their high aspect ratios and low surface area.[28] However, the carbon nanofillers unavoidably increase the dielectric loss and leakage conductivity loss of polymer sharply because of their high electrical conductivity. In order to resolve the limited chemical compatibility and aggregation of fillers in the polymer matrix, the filler dispersion can be improved *via* nanofiller surface modification by hydroxylation,[29] coupling agents,[30] surfactants,[31,32] phosphoric acids[33,34] and other organic molecules[35] in the polymer matrix. However, this surface modification approach always results in limited enhancements in permittivity due to the large volumes of the introduced inert surface layers.[36] Therefore, the challenge to simultaneously achieve enhanced permittivity, low loss and great mechanical reliability in the single-layered nanocomposites still remains.

Recently, topological structured composites have been widely applied in the field of electrical insulation and energy storage, which contain insulating layers to suppress dielectric loss as a result of the blocking effects of the interfaces between the neighboring layers.[37–39] We utilize the topological structures to develop flexible tri-layered-structured polymer films with enhanced permittivity, low loss, and great mechanical reliability. In these structures, acid-treated multi-walled carbon nanotubes (MWCNT) dispersed in ferroelectric poly(vinylidene fluoride-*co*-hexafluoropropene) (P(VDF-HFP)) matrix at the top and bottom of the composite act as two highly conductive layers to enhance permittivity, while the middle layer poly(methyl methacrylate) (PMMA)/P(VDF-HFP) blends can effectively suppress dielectric losses because the relaxation phenomenon of the ferroelectric copolymer can be mitigated by linear dielectric PMMA.[40,41] The acid-treated MWCNTs are homogenously and randomly dispersed in P(VDF-HFP) matrix assisted by the strong noncovalent interaction between the F atoms in polymer chains and the oxygen-containing groups on the surface of MWCNTs. Compared with previously reported works with similar values of permittivity, the tri-layered-structured films are proved to be more effective in lowering the packing ratio and suppressing dielectric loss due to the tight interfaces and chemical compatibility between adjacent layers. Composition optimization of the composites results in a greatly enhanced permittivity of 21 accompanied by a low dielectric loss of 0.05. Specifically, the nanocomposites are endowed with excellent mechanical flexibility and dielectric stability over rigorous winding and bending tests. These attractive features of the designed tri-layered nanocomposites indicate that the method proposed herein is a new approach for developing flexible composites with high permittivity and low dielectric loss.

2. Experimental section

2.1. Materials

MWCNTs were purchased from Beijing DK Nano technology Co. Ltd with the following specifications: 0.5–2.0 μm in length, 10–20 nm in diameter, >98 wt% purity with <1.5 wt% ash (Fig. 2(a) and (b)). P(VDF-HFP) was obtained from Arkema, with 10 wt% HFP and molecular weight of MW 530 000. Nitric acid was obtained from Guangzhou Chemical Reagent Co., Ltd. *N*,*N*-Dimethylformamide (DMF) with analytical purity was obtained from Letai Co., China.

2.2. Synthesis

Functionalization of MWCNTs. In a 500 mL round-bottom flask with a condenser, approximately 2 g of the as-received MWCNTs were dispersed in 200 mL 68% nitric acid. The dispersion was refluxed at 110 °C for 8 h. The resulting dispersion is then diluted and filtered with deionized water. The remaining solids were washed to achieve neutral pH, dried overnight at 120 °C in a vacuum, cooled to room temperature, then stored in a desiccator and labeled acid-treated MWCNTS.

Preparation of acid-treated-MWCNT/P(VDF-HFP) composite films. A series of acid-treated-MWCNT/P(VDF-HFP) composite films was prepared *via* the solution casting method with ultrasonication, with acid-treated-MWCNT concentrations ranging from 0 to 11.0 wt%. The method is as follows: firstly, the acid-treated MWCNT was dissolved in DMF and stirred at 30 °C for 12 h, and then P(VDF-HFP) powder was dissolved to form a uniform and stable blend suspension. Then, the stable suspension was cast on a clean glass plate with laboratory casting equipment (MSK-AFA-L800, Hefei Ke Jing Materials Technology Co., Ltd), and the solvent was completely evaporated after 10 hours of vacuum drying. Finally, the dried film was heated at 200 °C under vacuum for 5 min and then quenched in ice water immediately to obtain a dense composite film. The final quenched film is dried overnight at 60 °C, allowing the remaining water to evaporate completely and peel off from the glass substrate.

Fabrication of the tri-layered composites. Tri-layered structured films were prepared by the layer by layer solution casting method. The acid-treated MWCNT was first dissolved in DMF and stirred at 30 °C for 12 h, and then the powder of P(VDF-HFP) was dissolved to form a uniform and stable suspension. The powder of P(VDF-HFP) was dissolved in DMF and stirred at 30 °C for 12 h, and then PMMA particles were dissolved to obtain a uniform and stable blend solution. Then, a part of MWCNT/P(VDF-HFP) stabilized suspension was cast on clean glass plates using laboratory casting equipment and dried completely as the outer film after evaporation of solvent at 80 °C for 1 h. The inner layer of PMMA/P(VDF-HFP) blend

solution is then poured into the outer layer. Then, the remaining MWCNT/P(VDF-HFP) solution was cast into the middle layer as another outer layer. All the films were dried at 60 °C for 10 h, and the solvent evaporated completely. Finally, the dried film was heated at 200 °C vacuum for 5 min and then quenched in ice water immediately to obtain a dense three-layer structure film. To allow the residual water to evaporate completely, the final quenched film was dried overnight at 60 °C and peeled off from the glass substrate. By simply changing the concentration of the solution and the height of the scraper, the thickness of each layer in the three-layer structure film can be controlled. The cross-sections of all composite membranes were obtained by freezing fracture in liquid nitrogen, and the surface morphology was observed by scanning electron microscopy (SEM, Quanta 250FEG, FEI, Ltd). The image of MWCNT was obtained by transmission electron microscopy (TEM, 2100, JEOL, Ltd).

2.3. Characterization

For dielectric measurements, an automatic precision coating machine (JFC-1600, JEOL, LTD) was used to spout gold electrodes with a typical thickness of 100 nm and a diameter of 2 mm on both sides of the polymer film. The crystal structure was characterized by powder X-ray diffraction (XRD, SHIMADZU XRD-7000, Tokyo, Japan) with Cu Kα (1.5408 Å) in the 2θ range from 10 to 30°. Fourier transform infrared spectroscopy was conducted using a Nicolet iS50 (Thermo Fisher Scientific, USA) in the range of 600–1600 cm^{-1}, with a resolution of 4 cm^{-1}. At room temperature, dielectric properties and AC resistivity were measured using an impedance analyzer (4990A, Agilent Technologies, Inc.) at frequencies ranging from 1 kHz to 10 MHz. The mechanical bending test was carried out with a computer-aided self-made bending test system (as shown in Fig. 7a).

3. Results and discussion

3.1. Structural characterization of the tri-layered composite

The unmodified MWCNTs were oxidized in nitric acid (HNO_3). This process increases the defective sites and generates oxygen-containing groups on the surface of MWCNTs and hence enhances the reactivity of MWCNTs, as illustrated in Fig. 1a and b. Fig. 1b and Fig. S1 (ESI†) show the photographs of solution stability of the suspension with MWCNTs in DMF solution. The solution remained stable and dispersed in DMF solution over a month, confirming the –OH has been grafted onto the MWCNTs successfully.[42] The microscopic structures of MWCNTs were investigated by TEM as shown in Fig. 2a and b, and the diameter of the MWCNTs was about 10–20 nm. As shown in Fig. 2c, the surface chemical structures of MWCNTs oxidized by HNO_3 were further investigated by FTIR spectra. The wide absorption band at 1570–1700 cm^{-1} was attributed to MWCNTs. The broad band at 3420 cm^{-1} was in stretch mode O–H, which is caused by physically adsorbed water (OH).[43]

Then, P(VDF-HFP) powder was dissolved in the above MWCNTs/DMF solution, and the composite film was prepared by the simple ultra-sonication-assisted solution casting method. Fig. 1a and Fig. S2 (ESI†) show the optical images of the flexible and high-quality composite films (0.1%–11 wt%) with a large size of 5 × 6 cm. Further observing the cross-section SEM of the composite film (Fig. 2d), the acid-treated MWCNTs appeared as bright dots and were well dispersed and tightly embedded within the P(VDF-HFP) matrix. Such good compatibility of acid-treated MWCNTs with P(VDF-HFP) and quality of dispersion observed in SEM are related to the strong interactions. The H atoms provided by –OH group are positively charged, most likely indicating that H is able to have a strong noncovalent interaction with the F atoms in PVDF.

A series of tri-layered composites was prepared by sequentially casting three layers containing two outer layers with (7–11 wt%)

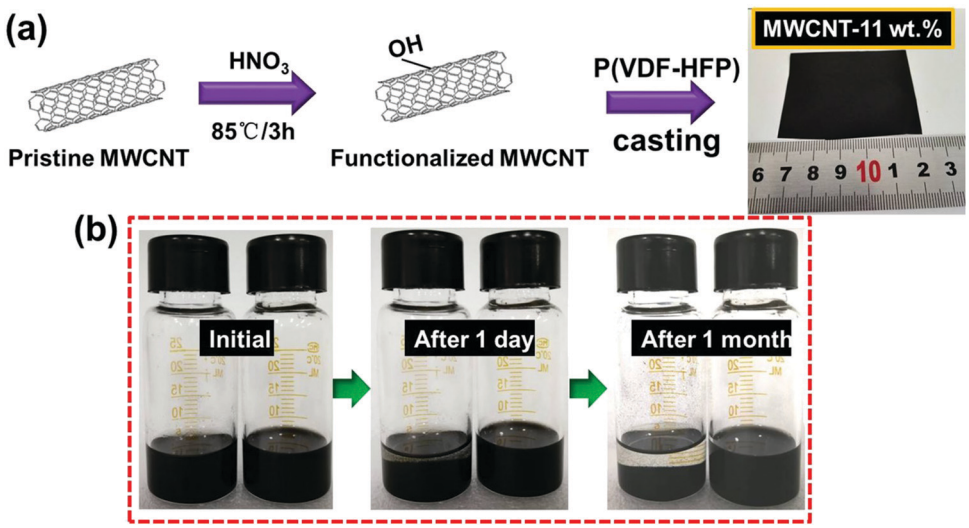

Fig. 1 (a) Schematic representation of the process by which CNTs are oxidized using acid and a photograph of the single layer film with 11 wt% MWCNT (b) Photographs of solution stability of the suspension with MWCNTs in DMF solution: left: untreated MWCNTs and right: acid-treated MWCNTs.

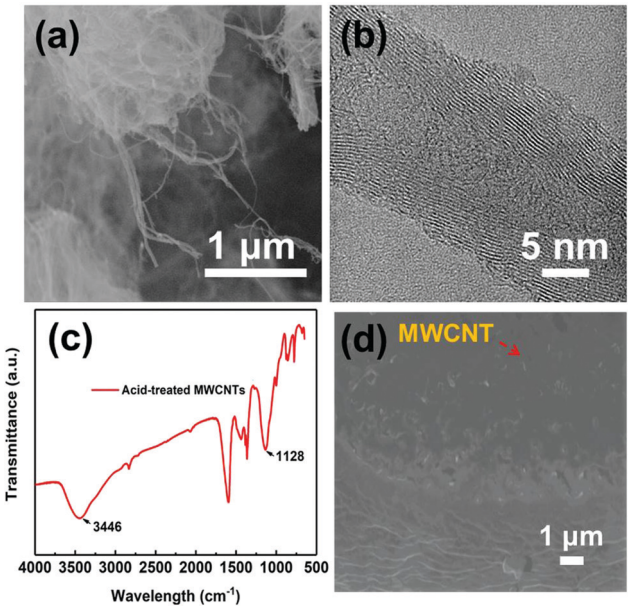

Fig. 2 (a) SEM images of MWCNTs. (b) TEM micrograph of MWCNTs. (c) FTIR spectra of acidified MWCNTs and (d) cross-section SEM image of MWNT/PVDF composite with MWCNT mass fraction of 7%.

acid-treated MWCNT contents and medium layer with PMMA (5 wt%). The succinct symbol of 7-5-7 has been used to represent the film with the acid-treated MWCNT mass fractions of 7, 9, and 11 wt% in the upper and bottom layers, and a fixed PMMA mass fraction of 5 wt% in middle layer. The microscopic morphologies, layer architecture and thicknesses of central layers and neighboring layers of the films were further investigated by the cross-section images, as shown in Fig. 3a. Due to the chemical compatible effect between the amorphous PMMA and semi-crystalline P(VDF-HFP), the interfaces were tightly integrated without visible pores and the presence of voids, thus leading to dense ternary tri-layer composite films.[44] The optical image of the flexible and high-quality ternary tri-layer composite film with a large size of 6 × 4 cm is presented in Fig. 3b.

3.2. Microstructure of the tri-layered composite

The XRD patterns of pure PVDF-HFP and tri-layered composite films are shown in Fig. 4. It can be seen that all these films exhibit peaks at 2θ =17.9, 18.4 and 20.2, which correspond to the α-phase,[45] and the broad peak at 26.6 corresponds to the

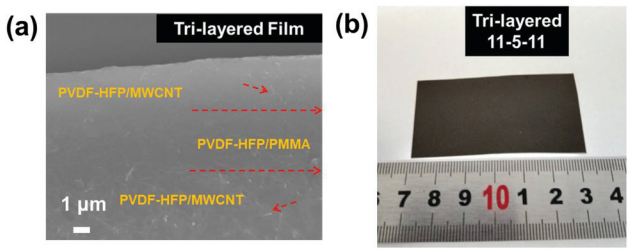

Fig. 3 (a) Cross-section SEM image of the tri-layered composite film with 11 wt% MWCNT and (b) a photograph of the tri-layered composite film.

superposition of the γ-phase diffraction. For the tri-layered composite system, the peak of the α-phase at 2θ =18.4 and 26.6 is weakened after the introduction of the MWCNTs. In the meantime, the diffraction peak is slightly shifted up at a 0.2° increment for the 11-5-11 sample. The FT-IR spectra in Fig. 4b also confirm the unvaried crystal phase. The characteristic absorption bands of the α-phase were detected at 1403 cm^{-1}, 1382 cm^{-1}, 1211 cm^{-1}, 1147 cm^{-1}, 974 cm^{-1}, 854 cm^{-1}, 795 cm^{-1} and 763 cm^{-1} in the ternary tri-layered architecture films and PVDF-HFP films.[46] And the peaks at 1234, 838 cm^{-1} correspond to γ-phase. No obvious peaks of β are detected.

3.3. Dielectric properties of the tri-layered composite

We firstly investigated the frequency dependence of the dielectric properties of the single layer MWCNT/P(VDF-HFP) composites, as plotted in Fig. S3 (ESI†). It is clear that the content of MWCNT plays a critical role in determining dielectric behaviors of composites. It is also worth noting that the dielectric properties of the MWNT/P(VDF-HFP) composites show similar trend over the whole frequency range (1 kHz to 10 MHz) as that of the pure P(VDF-HFP) below percolation threshold. A dielectric loss peak can be also observed at about 10 MHz (see Fig. S3b, ESI†), which may be attributed to the dielectric relaxation in the P(VDF-HFP) matrix.[47] Once above the percolation threshold, the variation of corresponding dielectric performance is very obvious. For instance, permittivity increased mildly, *i.e.* from 10 for pristine P(VDF-HFP) to 43.6 for composite with 7 wt% MWCNT at 1 kHz, while the dielectric loss is maintained at a low value (~0.079) in this measured frequency, which is also presented in Fig. S4a (ESI†). In stark contrast, with further increasing content of MWCNT, permittivity in the measured frequency range and corresponding dielectric loss increase obviously at 1 kHz for the 9 wt% and 11 wt% films. The abrupt changes in permittivity and dielectric loss may be primarily ascribed to the formed conductive network and larger leakage currents resulting from the higher conductivity when the filler content of the composites approaches the percolation threshold. These results have been verified by the data of frequency dependent alternate current (AC) conductivity, as shown in Fig. S4b (ESI†). The electrical conductivity in the composite film with 7 wt% MWCNT is 1.87 × 10^{-5} S m^{-1}, suggesting their favorable electrical insulation properties. Furthermore, the AC conductivity increases mildly to 3.07 × 10^{-5} S m^{-1} with the increase of the filler content to 9 wt%. In comparison, the higher conductivity (1.19 × 10^{-4} S m^{-1}) of the composite approaches the percolation threshold, which can be observed in the insert of Fig. S4b (ESI†).

Fig. 5a shows the permittivity of single layer and tri-layered architecture films as a function of frequency, over the range from 1 kHz to 10 MHz. With the increasing frequency, permittivity of all ternary tri-layered polymer films tends to decrease. It can be seen that significant increases in permittivity are observed with increasing MWCNT loading of the outer layer, while the dielectric loss remains at a low value (Fig. 5b) even for the composite approaching the percolation threshold. Apparently, all ternary tri-layered polymer films have much

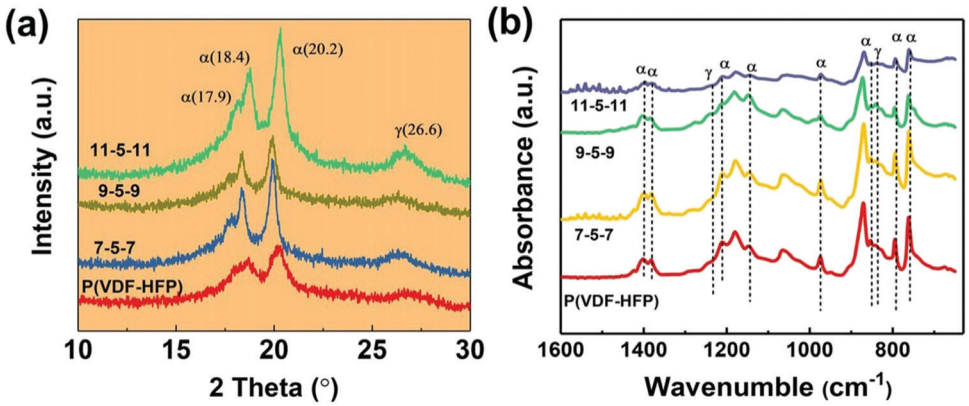

Fig. 4 (a) XRD pattern and (b) FT-IR spectra of pure P(VDF-HFP) and tri-layered composite films.

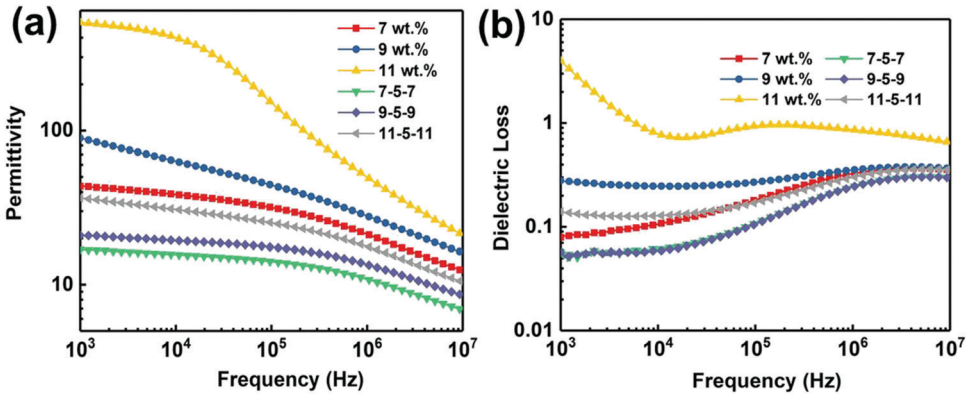

Fig. 5 (a) Dependence of the permittivity and (b) dielectric loss of the single layer and tri-layered composite films.

lower dielectric loss than single layer films with identical filler content over the whole frequency range (1 kHz to 10 MHz), which is important for film capacitor applications in preventing the self-heating of dielectrics. Fig. 6 shows the permittivity and dielectric loss of the single layer and tri-layered composite films at 1 kHz as a function of MWCNT content. The dielectric loss of the ternary tri-layered architecture film (11-5-11) is 0.14 even when the outer layer contains 11 wt% fillers at 1 kHz, while the dielectric loss of the single-layered film is 4. The low dielectric loss could be attributed to the following explanation: (i) the formation of hydrogen bonds could effectively promote the homogeneous distribution of MWCNT and the strong interfacial adhesion in the P(VDF-HFP) matrix, (ii) poly(methyl methacrylate) (PMMA)/P(VDF-HFP) blends can effectively suppress dielectric losses caused by linear dielectric PMMA mitigating the relaxation phenomenon of ferroelectric polymer, and

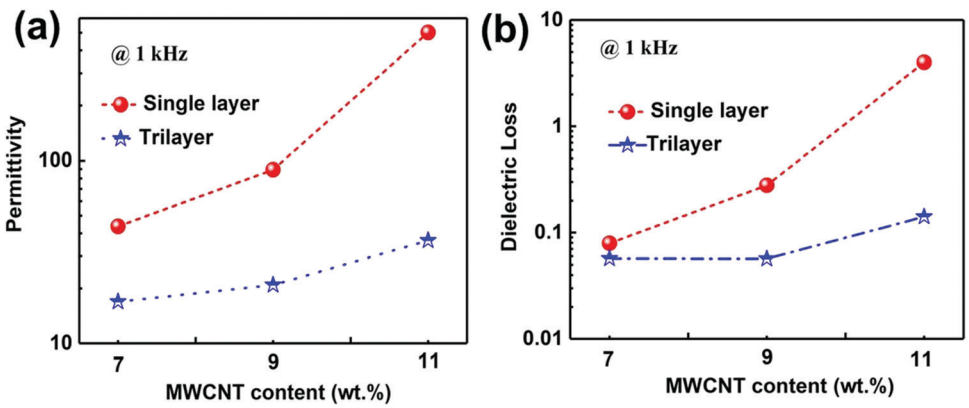

Fig. 6 (a) Permittivity and dielectric loss of the single layer and tri-layered composite films at 1 kHz as a function of MWCNT content.

Table 1 Comparisons of filler content, permittivity, dielectric loss and fabrication method for different composites

Nanocomposites	Filler content	Dielectric constant	Dielectric loss	Fabrication technique
BT-np/PVDF-CTFE ref. 34	50% (volume)	37 (1 kHz)	0.07	Ball-milled, spin-coating
BT-nw/PVDF ref. 48	10% (volume)	49 (100 Hz)	0.65	Ultra-sonication, solution-casting
Ni/PVDF ref. 49	27% (volume)	210 (1 kHz)	0.25	Physical blending, hot-press
CCTO/PVDF ref. 50	55% (volume)	77.5 (1 kHz)	0.11	Melt-mixed, hot-press
La-CCTO/PVDF ref. 51	10% (mass)	31 (100 Hz)	0.35	High temperature extrusion, hot-press
POSS@CNT/PVDF ref. 52	5% (mass)	50 (1 kHz)	0.7	Ultra-sonication, solution-casting
MWCNT/PVDF ref. 53	1.6% (volume)	50 (1 kHz)	0.4	Physical blending, hot-molding
MWCNT@SiO_2/PEN ref. 54	3% (mass)	8 (1 kHz)	0.06	Ultra-sonication, solution-casting
GO-e-CNT–PU ref. 55	5% (mass)	11 (1 kHz)	0.1	Ultra-sonication, hot-press
TiO_2@MWCNTs/PVDF ref. 56	0.1 (mass)	15 (1 kHz)	0.1	hydrothermal process, solution-casting
Tri-layered nanocomposite	**9% (mass)**	**21 (1 kHz)**	**0.05**	**Solution-casting**
This work	**11% (mass)**	**36.5 (1 kHz)**	**0.14**	**Solution-casting**

BT: barium titanate $BaTiO_3$; MWCNT: multi-walled carbon nanotubes; POSS: polyhedral oligomeric silsesquioxane; PEN: poly(arylene ether nitrile); GO-e-CNT: graphene oxide-encapsulated carbon nanotube; PU: polyurethane.

(iii) due to the chemical compatibility and tight interfaces between adjacent layers, the tri-layered-structured films have been more effective in suppressing dielectric loss in comparison with single layer composites with an identical content of MWCNT.

For comparison with the dielectric capabilities of other previously reported polymer composites, the corresponding filler content, permittivity, dielectric loss and fabrication process are listed in Table 1.[48–56] Obviously, high permittivity can be obtained in single layer composites introduced with BT, CCTO and Ni. However, these composites, due to high filler content in composites with ceramic nanofiller and high dielectric loss in percolative composites, have several inevitable drawbacks, such as poor mechanical flexibility and overheating. In particular, higher permittivity can be obtained in the tri-layered composite film when compared with most of the nanocomposites based on MWCNTs as fillers. It is shown that the tri-layered composite film with a low filler content manifests high permittivity, low dielectric loss, and great mechanical flexibility, which is realized *via* a simple ultrasonication-assisted solution-casting method.

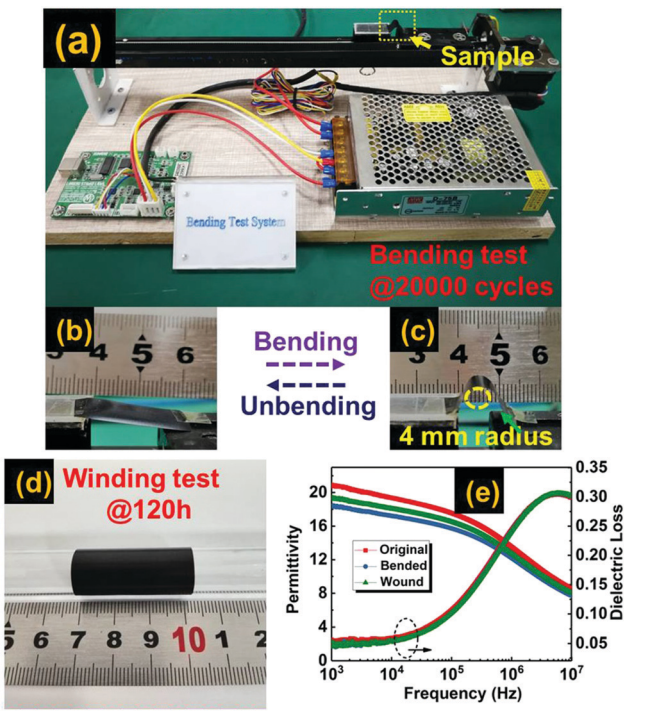

Fig. 7 Digital photographs of (a) experimental setup of the bending test. (b) One unbending and (c) bending cycle. (d) Tri-layered composite wrapped on a glass tube with 2 mm diameter for three turns. (e) Dielectric stability of tri-layered composite before and after winding and bending tests.

3.4. Mechanical durability of the tri-layered composite

The mechanical flexibility and robustness against bending deformations of dielectric materials are important abilities of wound film capacitor cells.[57,58] In order to demonstrate the mechanical flexibility and durability of the tri-layered composite, the winding test is adopted, in which a tri-layered film strip is wrapped on a glass tube with 2 mm diameter and the coiled state is held for 120 hours, as shown in Fig. 7(d). The second test is the bending test, in which we bend and unbend a tri-layered film strip repeatedly at a bending curvature of 4 mm radius over straight 20 000 cycles. Each cycle is programmed to be accomplished in 5 seconds, as plotted in Fig. 7(a)–(c). The dielectric stability of the wound and bended samples was investigated by frequency dependent dielectric properties. The results of Fig. 7(e) indicate that both the wound and bended samples possess dielectric properties similar to those of the original material.

4. Conclusions

In summary, construction of a ternary tri-layered structure film with excellent dielectric properties and mechanical endurance is reported, which is composed of two outer layers of acid-treated MWCNT dispersed in the P(VDF-HFP) matrix and a middle layer of PMMA dispersed in the P(VDF-HFP) matrix by a facile layer-by-layer solution-casting technique. Owing to the successful formation of hydroxylation of MWCNTs, the composite powder can be uniformly dispersed in the matrix of P(VDF-HFP). Consequently, the tri-layered-structure nanocomposites with tight interfaces are capable of balancing the

contradicted parameters, including permittivity, dielectric loss, and mechanical reliability, to endow excellent capacitive performance exceeding those of previously reported polymer dielectrics. The ternary tri-layered film with an optimized filler content (9 wt%) exhibited a high permittivity of 21 and a quite low dielectric loss of 0.05. Moreover, the results of mechanical tests (including bending and winding) show that the composite retained mechanical flexibility and capacitor stability after rigorous cycles. Therefore, such multilayer structure composites with functional fillers have potential applications in film capacitors due to ease of processability, good flexibility, high permittivity, and low dielectric loss.

Conflicts of interest

There are no conflicts to declare.

Acknowledgements

H. W. acknowledges the support of Shezhen Science and Technology Program (No. KQTD20180411143514543 and JCYJ20180504165831308) and Shenzhen DRC project [2018]1433.

References

1 C. W. Nan, Y. Shen and J. Ma, *Annu. Rev. Mater. Res.*, 2010, **40**, 131.
2 Y. Wu, X. Y. Lin, X. Shen, X. Y. Sun, X. Liu, Z. Y. Wang and J. K. Kim, *Carbon*, 2015, **89**, 102–112.
3 Z. M. Dang, J. K. Yuan, S. H. Yao and R. J. Liao., *Adv. Mater.*, 2013, **25**, 6334–6365.
4 B. C. Luo, X. H. Wang, Y. P. Wang and L. T. Li, *J. Mater. Chem. A*, 2014, **2**, 510–519.
5 Y. Zhao, Q. Liao, G. Zhang, Z. Zhang, Q. Liang, X. Liao and Y. Zhang, *Nano Energy*, 2015, **11**, 719–727.
6 H. Luo, X. F. Zhou, C. Ellingford, Y. Zhang, S. Chen, K. C. Zhou, D. Zhang, C. R. Bowen and C. Y. Wan, *Chem. Soc. Rev.*, 2019, **48**, 4424–4465.
7 H. Luo, S. Chen, L. H. Liu, X. F. Zhou, C. Ma, W. W. Liu and D. Zhang, *ACS Sustainable Chem. Eng.*, 2019, **7**, 3145–3153.
8 Y. Lin, C. Sun, S. L. Zhan, Y. J. Zhang and Q. B. Yuan, *Adv. Mater. Interfaces*, 2020, 2000033.
9 X. J. Zhang, G. S. Wang, Y. Z. Wei, L. Guo and M. S. Cao, *J. Mater. Chem. A*, 2013, **1**, 12115–12122.
10 Y. Feng, W. L. Li, J. P. Wang, J. H. Yin and W. D. Fei, *J. Mater. Chem. A*, 2015, **3**, 20313–20321.
11 H. Tang and H. A. Sodano, *Nano Lett.*, 2013, **13**, 1373–1379.
12 Y. Wang, X. Zhou, Q. Chen, B. Chu and Q. Zhang, *IEEE Trans. Dielectr. Electr. Insul.*, 2010, **17**, 1036.
13 Y. Q. Chen, B. P. Lin, X. Q. Zhang, J. C. Wang, C. W. Lai, Y. Sun, Y. R. Liu and H. J. Yang, *J. Mater. Chem. A*, 2014, **2**, 14118–14126.
14 F. X. Guan, J. Wang, J. L. Pan, Q. Wang and L. Zhu, *Macromolecules*, 2010, **43**, 6739–6748.
15 W. M. Xia, Z. Xu, F. Wen, W. J. Li and Z. C. Zhang, *Appl. Phys. Lett.*, 2010, **97**, 222905.
16 C. C. Wang, J. X. Zhang, S. B. Gong and K. L. Ren, *J. Appl. Phys.*, 2018, **124**, 154103.
17 S. D. Liao, Z. H. Shen, H. Pan, X. Zhang, Y. Shen, Y. H. Lin and C. W. Nan, *J. Mater. Chem. C*, 2017, **5**, 12777.
18 Y. F. Wang, J. Chen, Y. Li, Y. J. Niu, Q. Wang and H. Wang,, *J. Mater. Chem. A*, 2019, **7**, 2965.
19 Y. J. Niu, Y. Bai, K. Yu, Y. Wang, F. Xiang and H. Wang, *ACS Appl. Mater. Interfaces*, 2015, **7**, 24168–24176.
20 Y. Song, Y. Shen, P. H. Hu, Y. H. Lin, M. Li and C. W. Nan, *Appl. Phys. Lett.*, 2012, **101**, 152904.
21 S. H. Liu, S. X. Xue, W. Q. Zhang, J. W. Zhai and G. H. Chen, *J. Mater. Chem. A*, 2014, **2**, 18040.
22 J. Y. Li, L. Zhang and S. Ducharme, *Appl. Phys. Lett.*, 2007, **90**, 132901.
23 K. Meeporn and P. Thongbai, *Appl. Surf. Sci.*, 2019, **481**, 1160–1166.
24 W. Y. Li, Z. Q. Song, J. M. Zhong, J. Qian, Z. Y. Tan, X. Y. Wu, H. Y. Chu, W. Nie and X. H. Ran, *J. Mater. Chem. C*, 2019, **7**, 10371–10378.
25 L. K. Wu, W. F. Yuan, N. Hu, Z. C. Wang, C. L. Chen, J. H. Qiu, J. Ying and Y. Li, *J. Phys. D: Appl. Phys.*, 2014, **47**, 135302.
26 E. Francis, H. U. Ko, J. W. Kim, H. C. Kim, N. Kalarikkal, K. Varughese, J. Kim and S. Thomas, *J. Mater. Chem. C*, 2018, **6**, 8152.
27 W. Y. Li, Z. Q. Song, J. Qian, Z. Y. Tan, H. Y. Chu, X. Y. Wu, W. Nie and X. H. Ran, *Carbon*, 2019, **141**, 728–738.
28 Z. M. Dang, M. S. Zheng and J. W. Zha, *Small*, 2016, **12**, 1688–1701.
29 J. J. Li, S. I. Seok, B. J. Chu, F. Dogan, Q. M. Zhang and Q. Wang, *Adv. Mater.*, 2009, **21**, 217.
30 X. Y. Huang, L. Y. Xie, K. Yang, C. Wu, P. K. Jiang, S. T. Li, S. Wu, K. Tatsumi and T. Tanaka, *IEEE Trans. Dielectr. Electr. Insul.*, 2014, **21**, 480.
31 H. Tang, Y. Lin and H. A. Sodano, *Adv. Energy Mater.*, 2013, **3**, 451.
32 J. J. Li, P. Khanchaitit, K. Han and Q. Wang, *Chem. Mater.*, 2010, **22**, 5350.
33 P. Kim, S. Jones, P. Hotchkiss, J. Haddock, B. Kippelen, S. Marder and J. Perry, *Adv. Mater.*, 2007, **19**, 1001.
34 P. Kim, N. M. Doss, J. P. Tillotson, P. J. Hotchkiss, M. J. Pan, S. R. Marder, J. Y. Li, J. P. Calame and J. W. Perry, *ACS Nano*, 2009, **3**, 2581.
35 P. H. Hu, Y. Shen, Y. H. Guan, X. H. Zhang, Y. H. Lin, Q. M. Zhang and C. W. Nan, *Adv. Funct. Mater.*, 2014, **24**, 3172.
36 X. Huang and P. K. Jiang, *Adv. Mater.*, 2015, **27**, 546–554.
37 Y. F. Wang, L. X. Wang, Q. B. Yuan, J. Chen, Y. J. Niu, X. W. Xu, Y. T. Cheng, B. Yao, Q. Wang and H. Wang, *Nano Energy*, 2018, **44**, 364–370.
38 Y. F. Feng, Q. Wu, Q. H. Deng, C. Peng, J. B. Hu and Z. C. Xu,, *J. Mater. Chem. C*, 2019, **7**, 6744.
39 H. J. Ye, X. H. Zhang, C. F. Xu, B. Han and L. X. Xu, *J. Mater. Chem. C*, 2018, **6**, 11144–11155.
40 Y. Cui, X. Wang, T. D. Zhang, C. H. Zhang and Q. G. Chi, *RSC Adv.*, 2019, **9**, 33229.

41 B. C. Luo, X. H. Wang, H. X. Wang, Z. M. Cai and L. T. Li,, *Compos. Sci. Technol.*, 2017, **151**, 94–103.
42 S. W. Kim, T. Kim, Y. S. Kim, H. S. Choi, H. J. Lim, S. J. Yang and C. R. Park, *Carbon*, 2012, **50**, 3–33.
43 W. Yan, Y. Zhang, H. W. Sun, S. W. Liu, Z. G. Chi, X. D. Chen and J. R. Xu,, *J. Mater. Chem. A*, 2014, **2**, 20958.
44 J. Chen, Y. F. Wang, Q. B. Yuan, X. W. Xu, Y. J. Niu, Q. Wang and H. Wang, *Nano Energy*, 2018, **54**, 288–296.
45 X. Lin, P. H. Hu, Z. Y. Jia and S. M. Gao, *J. Mater. Chem. A*, 2016, **4**, 2314–2320.
46 C. L. Liang, Z. H. Mai, Q. Xie, R. Y. Bao, W. Yang, B. H. Xie and M. B. Yang, *J. Phys. Chem. B*, 2014, **118**, 9104–9111.
47 R. Rama, M. Rahaman and D. Khastgir, *Composites, Part A*, 2015, **69**, 30–39.
48 Y. Feng, W. L. Li, Y. F. Hou, Y. Yu, W. P. Cao, T. D. Zhang and W. D. Fei, *J. Mater. Chem. C*, 2015, **3**, 1250–1260.
49 M. Panda, V. Srinivas and A. K. Thakur, *Appl. Phys. Lett.*, 2008, **92**, 132905.
50 P. Thomas, K. T. Varughese, K. Dwarakanath and K. B. R. Varma, *Compos. Sci. Technol.*, 2010, **70**, 539–545.
51 A. Srivastava, P. Maiti, D. Kumar and O. Parkash, *Compos. Sci. Technol.*, 2014, **93**, 83–89.
52 W. J. Zhang, Z. Z. Zhou, Q. F. Li and G. X. Chen, *Ind. Eng. Chem. Res.*, 2014, **53**, 6699–6707.
53 L. Wang and Z. M. Dang, *Appl. Phys. Lett.*, 2005, **87**, 042903.
54 F. Jin, M. N. Feng, X. Huang, C. Long, K. Jia and X. B. Liu, *Appl. Surf. Sci.*, 2015, **357**, 704–711.
55 C. Wu, X. Y. Huang, X. F. Wu, L. Y. Xie, K. Yang and P. K. Jiang, *Nanoscale*, 2013, **5**, 3847–3855.
56 L. Yang, J. H. Qiu, H. L. Ji, K. J. Zhu and J. Wang, *Composites, Part A*, 2014, **65**, 125–134.
57 Q. Li, L. Chen, M. R. Gadinski, S. H. Zhang, G. Z. Zhang, H. Y. Li, A. Haque, L. Q. Chen, T. Jackson and Q. Wang, *Nature*, 2015, **523**, 576.
58 Z. Wang, T. Wang, C. Wang, Y. J. Xiao, P. P. Jing, Y. F. Cui and Y. P. Pu, *ACS Appl. Mater. Interfaces*, 2017, **9**, 29130–29139.